



Saltwater intrusion into the Changjiang River: A model-guided mechanism study

Pengfei Xue,¹ Changsheng Chen,^{1,2,3,4} Pingxing Ding,⁵ Robert C. Beardsley,⁶
Huichan Lin,¹ Jianzhong Ge,⁵ and Yazhen Kong⁵

Received 26 March 2008; revised 18 October 2008; accepted 3 December 2008; published 12 February 2009.

[1] The Changjiang River (CR) is divided into a southern branch (SB) and a northern branch (NB) by Chongming Island as the river enters the East China Sea. Observations reveal that during the dry season the saltwater in the inner shelf of the East China Sea flows into the CR through the NB and forms an isolated mass of saltwater in the upstream area of the SB. The physical mechanism causing this saltwater intrusion has been studied using the high-resolution unstructured-grid Finite-Volume Coastal Ocean Model (FVCOM). The results suggest that the intrusion is caused by a complex nonlinear interaction process in relation to the freshwater flux upstream, tidal currents, mixing, wind, and the salt distribution in the inner shelf of the East China Sea. The tidal rectification, resulting from the interaction of the convergence or divergence of tidal momentum flux and bottom friction over abrupt topography, produces a net upstreamward volume flux from NB to SB. With river discharge the net water transport in the NB is driven through a momentum balance of surface elevation gradient forcing, horizontal advection, and vertical diffusion. In the dry season, reducing the surface elevation gradient forcing makes tidal rectification a key process favorable for the saltwater intrusion. A northerly wind tends to enhance the saltwater intrusion by reducing the seaward surface elevation gradient forcing rather than either the baroclinic pressure gradient forcing or the wind-driven Ekman transport. A convergence experiment suggests that high grid resolution (~ 100 m or less) is required to correctly resolve the net water transport through the NB, particularly in the narrow channel on the northern coast of Chongming Island.

Citation: Xue, P., C. Chen, P. Ding, R. C. Beardsley, H. Lin, J. Ge, and Y. Kong (2009), Saltwater intrusion into the Changjiang River: A model-guided mechanism study, *J. Geophys. Res.*, 114, C02006, doi:10.1029/2008JC004831.

1. Introduction

[2] The Changjiang River (CR), one of the largest estuaries in the world, is a major freshwater source to the western Pacific Ocean [Chen *et al.*, 1994]. With an annual discharge rate of $\sim 3.0 \times 10^4$ m³/s and a maximum rate of $> 8 \times 10^4$ m³/s, this river counts for 90% of the total freshwater content in the East China Sea [Beardsley *et al.*, 1985]. In the past 20 years, research on the CR has focused on its impact on the salt balance and circulation in the East China Sea [Beardsley *et al.*, 1985; Chen *et al.*, 1994, 2008a]. One reason for this

focus was that in the past the CR was characterized as a homogeneous estuary occupied fully with freshwater in both dry and wet seasons (the dry and wet seasons refer to the winter and summer seasons with small and large freshwater discharges), and its interaction with seawater generally took place in the inner shelf of the East China Sea. For example, the seasonal variability of the Changjiang Diluted Water plume, which forms as a result of mixing between a large amount of freshwater discharge, tides and wind off the CR, directly contributes to the broad-scale adjustment of the East China Sea circulation and water flux into the surrounding regional oceans [Chen *et al.*, 2008a].

[3] Our understanding, however, is challenged by recent observations of saltwater intrusions into the CR [Mao and Shen, 1995; Xiao and Shen, 1998; Mao *et al.*, 2001; Kong *et al.*, 2004; He *et al.*, 2006]. The CR is a typical tidal estuary characterized by abrupt bathymetry, islands, and deep channels [Chen *et al.*, 2008a]. Chongming Island, located in the river mouth, divides the CR into southern and northern branches (Figure 1). The southern branch (hereafter referred to as SB) follows the mainstream of the CR discharge, is ~ 10 – 20 km wide, and connects to the East China Sea through three deep passages (with a water depth of ~ 20 m), while the northern branch (hereafter referred to as NB) is like a funnel

¹School for Marine Science and Technology, University of Massachusetts-Dartmouth, New Bedford, Massachusetts, USA.

²Also at State Key Laboratory for Estuarine and Coastal Research, East China Normal University, Shanghai, China.

³Also at Department of Physical Oceanography, Woods Hole Oceanographic Institution, Woods Hole, Massachusetts, USA.

⁴Also at Marine Ecosystem and Environmental Laboratory, Shanghai Ocean University, Shanghai, China.

⁵State Key Laboratory for Estuarine and Coastal Research, East China Normal University, Shanghai, China.

⁶Department of Physical Oceanography, Woods Hole Oceanographic Institution, Woods Hole, Massachusetts, USA.

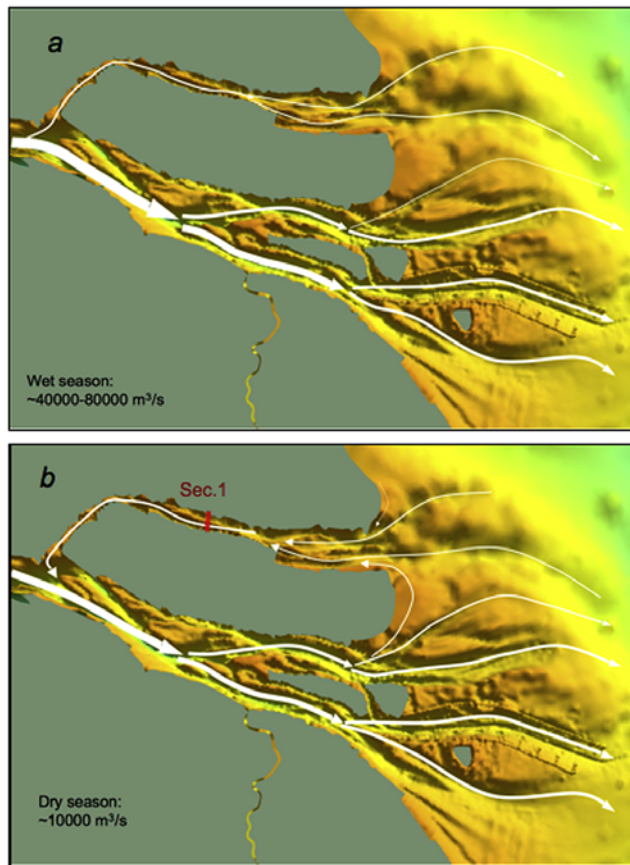


Figure 1. Three-dimensional bathymetry of the Changjiang River mouth and adjacent inner shelf region. The white curves show schematics of the subtidal flow patterns suggested by previous hydrographic measurements during the (a) wet and (b) dry seasons [Mao *et al.*, 2001; Kong *et al.*, 2004]. The red line in Figure 1b is the section selected for the momentum balance analysis shown in Figure 9. The bathymetric data used here are provided by the East China Normal University, which is constructed using both navigation maps and recent shipboard measurements.

with a width narrowing from ~ 10 km in the downstream area to ~ 2 km at the upstream entrance perpendicular to the SB. As a result of coastal construction and sedimentation, the coastal geometry and bathymetry in the NB have changed dramatically since the 1990s. The NB now features numerous intertidal zones, and with water depths in a range of ~ 1 – 8 m, is much shallower than the SB. Recent hydrographic measurements have detected saltwater in the upstream area of the SB [Mao and Shen, 1995; Xiao and Shen, 1998; Kong *et al.*, 2004; He *et al.*, 2006]. An example can be seen in the salinity measurements averaged over tidal cycles at anchor sites and recorded from in situ shipboard surveys on an along-river transect in the SB during spring and neap tidal cycles on 13–22 February 2004 (Figure 2) [Kong *et al.*, 2004; He *et al.*, 2006]. A tidally averaged salinity of ~ 2 was observed at Chongtou ($\sim 121.2^\circ\text{E}$, 31.75°N) around the northwestern headland of Chongming Island, forming a saltwater bore in the SB (Figure 2b). The salt content and location resulting from such a saltwater intrusion is related to the total freshwater transport of the CR, tidal amplitudes, and winds, with

maximum intrusion occurring usually during spring tide under low freshwater transport and northerly wind conditions [Kong *et al.*, 2004; Luo and Chen, 2006]. The 2004 salinity measurement showed a salinity peak of >3.5 at the intersection region of the SB and NB during the spring tide, while the peak dropped to ~ 1.0 and moved seaward during the neap tide (Figure 2c). This abnormal distribution of salinity observed inside the CR has turned this river into a stratified estuarine system with an energetic interaction with the seawater over the inner shelf.

[4] This salting tendency of the CR water has received intense attention in both economic and scientific aspects. The CR is a key freshwater source for Shanghai (the largest city in

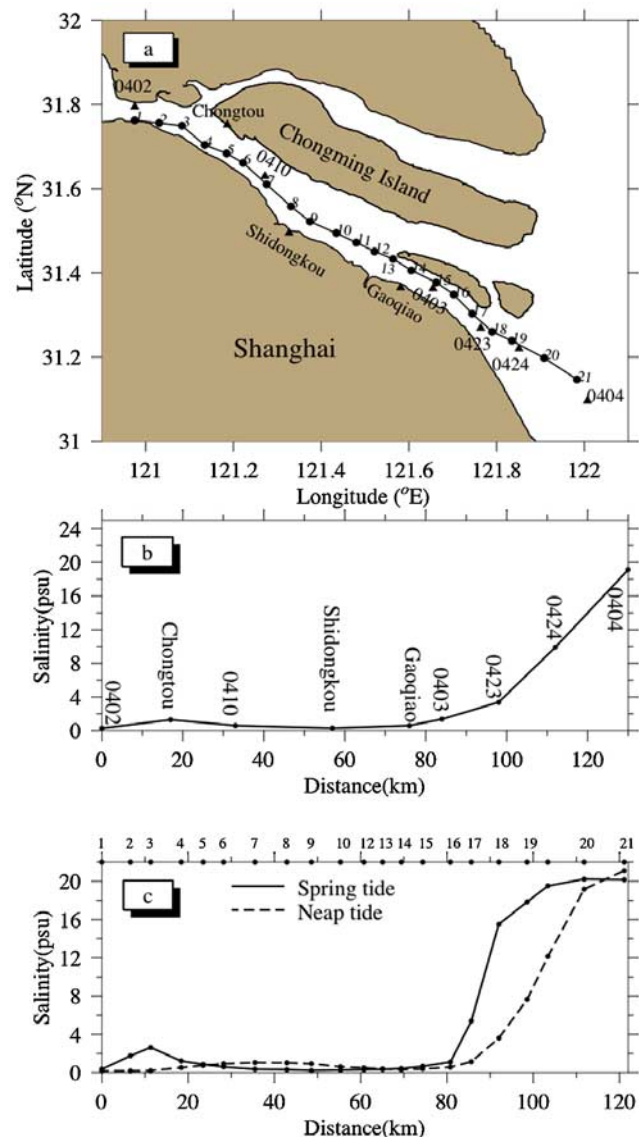


Figure 2. Distribution of the salinity measured from either anchor sites or shipboard surveys in the Changjiang River during 13–22 February 2004. (a) Locations of sampling stations with triangles for anchor sites and dots for shipboard survey sites. (b) Tidally averaged along-river distribution of salinity at anchor sites. (c) Along-river distribution of salinity along the ship track from stations 1 to 21 in surveys taken during spring and neap tides, respectively.

China) and surrounding regions. Changhai Reservoir, which connects to the SB of the CR and functions as the second largest freshwater supply for Shanghai, has had difficulty in providing high-quality freshwater during the dry season as a result of the recent salting of the CR water [Kong *et al.*, 2004]. In 1999, for example, the total freshwater transport from upstream was 9800, 9100 and 10,300 m³/s in January, February and March, respectively. During that period, salinity in the NB was up to 24–26. After the saltwater intruded into the SB and entered the Changhai Reservoir, the reservoir failed to provide drinking water to Shanghai for ~25 days [Mao *et al.*, 2001]. This situation has become much worse in recent years as a result of rapid increase of the economy around the downstream area of the CR [He *et al.*, 2006]. The saltwater intrusion into the CR also raises a fundamental question about the physical mechanism or mechanisms governing transport around a big island in a river. It is clear from the field measurements that the geometric difference between the NB and SB around Chongming Island provides a prerequisite geographic condition for the saltwater intrusion and the dynamic forcing causing this event is related to the change of upstream freshwater transport, tidal amplitudes and phases, and wind direction and intensity. However, it is unclear how these physical processes interact in this complex geometry to produce a northward net transport in the NB around Chongming Island. Are these processes equally important or does one of them play an essential role?

[5] Several modeling efforts have been made on simulating the saltwater intrusion process in the CR. Examples include Xiao *et al.* [2000], Luo and Chen [2005], Li *et al.* [2005], Ma *et al.* [2006], and Wu and Zhu [2007]. All of these studies were made using either 2-D or 3-D structured-grid (finite difference) models (which poorly resolved the complex coastal geometry around Chongming Island) and did not explore in detail the physical mechanism or mechanisms causing the saltwater intrusion. The saltwater intrusion into the CR depends critically on the net water transport in the NB. Accurate estimation of the transport requires a model to resolve the spatial/temporal structure of the water currents and water level over complex irregular coastal geometry and abrupt-varying bathymetry inside both NB and SB as well as around the river mouth. In addition to the need for a high-resolution model approach, we also require a better fitting of the coastal geometry of the CR with inclusion of Chongming Island. Failure to adequately resolve these geometric features can significantly underestimate the nonlinear interactions of physical forcings in this system, and thus makes it difficult to estimate the relative contribution of various physical processes to the saltwater intrusion into the CR.

[6] We, an international cooperative research team of the University of Massachusetts-Dartmouth (UMASSD), East China Normal University (ECNU) and Woods Hole Oceanographic Institution (WHOI), have applied the unstructured-grid, Finite-Volume Coastal Ocean Model (FVCOM) to the East China Sea (ECS) [Chen *et al.*, 2008a]. Here we have nested FVCOM-ECS to a high-resolution subdomain FVCOM of the CR (called FVCOM-CR) and used this new model to investigate the saltwater intrusion into this river. The unstructured-grid finite-volume approach used in FVCOM guarantees local mass and tracer conservation in the complex CR estuarine system, which makes it capable of simulating accurately the net transport in the NB under

different physical forcing environments and also tracing salt water in long-term simulations.

[7] In this paper, we describe the development of FVCOM-CR and its application to examine the strongly nonlinear processes of freshwater transport, tides and winds that cause the saltwater intrusion into the CR. Lagrangian and tracer experiments were first made for both wet and dry season physical conditions to “simulate” water transport in the CR and then an idealized process-oriented study was carried out to identify and qualify the relative importance of tidal rectification, freshwater transport and winds to cause the seawater intrusion in the NB. A sensitivity analysis was done to examine the influence of model resolution on the simulation results.

[8] This paper is organized as follows. FVCOM-CR and the design of the numerical experiments are described in section 2. The process-oriented model results under different physical conditions are presented in section 3. Physical mechanisms of saltwater intrusion through the NB are explored in section 4. A discussion follows in section 5 and the conclusions are summarized in section 6.

2. FVCOM-CR and Design of the Experiments

[9] FVCOM is an unstructured-grid, finite-volume, three-dimensional (3-D) primitive equation coastal ocean model developed by a joint effort of the University of Massachusetts-Dartmouth and Woods Hole Oceanographic Institution [Chen *et al.*, 2003, 2006a, 2006b, 2007, 2008a, 2008b, 2008c]. FVCOM is cast in a generalized terrain-following coordinate system [Pietrzak *et al.*, 2002] in the vertical and in control volumes consisting of unstructured triangular meshes in the horizontal. The spatial fluxes of momentum are discretized using a second-order accurate finite-volume method [Kobayashi *et al.*, 1999]. A flux formulation for scalars (e.g., temperature, salinity) is used in conjunction with a vertical velocity adjustment to enforce exact conservation of the scalar quantities. A Smagorinsky formulation [Smagorinsky, 1963] is used to parameterize the horizontal diffusion and turbulent vertical mixing is calculated using the General Ocean Turbulence Model (GOTM) libraries [Burchard, 2002], with the 2.5 level Mellor and Yamada [1982] turbulence model used as the default. The ability of FVCOM to accurately solve scalar conservation equations combined with the topological flexibility provided by unstructured meshes makes it ideally suited for the CR. A detailed description of FVCOM was given in the user manual that is available in the FVCOM Web site for registered users [Chen *et al.*, 2006a, 2006b].

[10] The high-resolution FVCOM-CR was developed by configuring the updated code of FVCOM to the CR with inclusion of the wet/dry treatment to intertidal zones. The computational domain of this model covers the CR, Hangzhou Bay, Zhoushan Island Complex, and is bounded by an open boundary in the inner shelf of the East China Sea (Figure 3). The horizontal resolution (measured by the shortest line of a triangle) varies from 0.1 to 0.5 km inside the CR and over the Zhoushan Island Complex to 1.0–3.0 km in Hangzhou Bay and 10.0 km in the inner shelf closest to the open boundary. The vertical resolution is determined by 10 uniform sigma layers, which is ~0.1 m or less over the intertidal zone and ~2.0 m in the inner shelf. The FVCOM-CR is driven by tidal

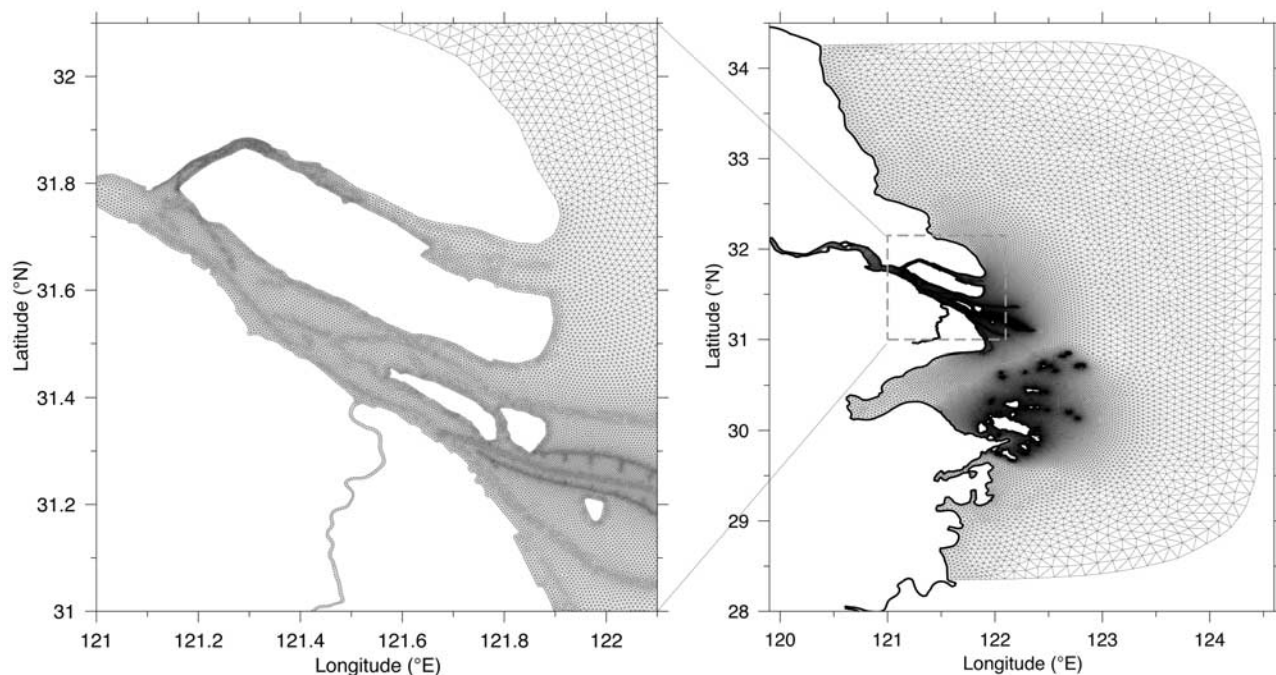


Figure 3. Unstructured grid of FVCOM-CR. Dashed line is the location of the open boundary that is nested to the FVCOM-ECS. The left panel provides an enlarged view of the grid inside the NB and SB.

elevation at the open boundary through nesting to FVCOM-ECS (with inclusion of four major tidal constituents: M_2 , S_2 , K_1 , and O_1), freshwater transport at the upstream end of the CR, and given winds that characterize the dry and wet seasons. The external and internal mode time steps were 1.0 and 10.0 s, which took about 15 min on a 16-node Linux cluster to integrate for a M_2 tidal cycle. The configuration of FVCOM-ECS was given in detail in the work of *Chen et al.* [2008a] and also on the UMASSD Web site <http://fvcom.smast.umassd.edu>.

[11] Four numerical experiments were conducted as case studies to identify the relative importance of various physical processes to the net transport into the NB of the CR during the wet and dry seasons. The configuration of these experiments is summarized in Table 1. In detail:

[12] Experiment 1 (Ex1): The model was driven by tidal forcing and freshwater transport of 60,000 m^3/s with a background initial salinity of 35 everywhere in the computational domain. The freshwater transport given in this case represents the wet season condition.

[13] Experiment 2 (Ex2): The model was run with the same tidal forcing and background initial salinity condition as those in Ex 1 but with a smaller freshwater transport of 10,000 m^3/s to represent the dry season condition.

[14] Experiment 3 (Ex3): The model was first run using Ex 1 conditions for 60 days and then restarted with the

freshwater transport of Ex2 for an additional 60-day integration. This case was aimed at examining the transition in transport process from the wet season to the dry season under the same tidal forcing condition.

[15] Experiment 4 (Ex4): The model was run with the same tidal, freshwater transport and background initial salinity conditions as Ex3 but with the addition of a northerly wind of 5 m/s. This case was designed to quantify the contribution of the wind to the intensity of the saltwater intrusion in the NB from the wet season to the dry season.

[16] In Ex1 and Ex2, we also tracked Lagrangian particles and dye concentrations released at different locations in the NB and SB. These experiments were aimed at examining the contributions of the Lagrangian flow field and mixing to the saltwater intrusion in the NB during the wet and dry seasons.

[17] To examine the physical mechanism or mechanisms that drive a northward net water transport into the NB, we have run the model with (1) only tidal forcing and (2) only freshwater discharge and compared the tidal rectified flow with the buoyancy-driven flow under both wet and dry conditions shown in Ex1 and Ex2. A momentum balance analysis was conducted for these cases to quantify the key physical process that causes the saltwater intrusion.

[18] We hypothesize that both coastline geometric fitting and horizontal resolution play a key role in resolving accurately

Table 1. Summary of Configurations of Four Numerical Experiments

Experiment	Case Type	Tides	Freshwater Discharge (m^3/s)	Winds	Initial Salinity (PSU)	Particle Tracking	Tracer Tracking
1	wet	yes	60,000	no	35	yes	no
2	dry	yes	10,000	no	35	yes	yes
3	wet to dry	yes	60,000–10,000	no	restart from 1	no	yes
4	wet to dry	yes	60,000–10,000	yes	restart from 1	no	no

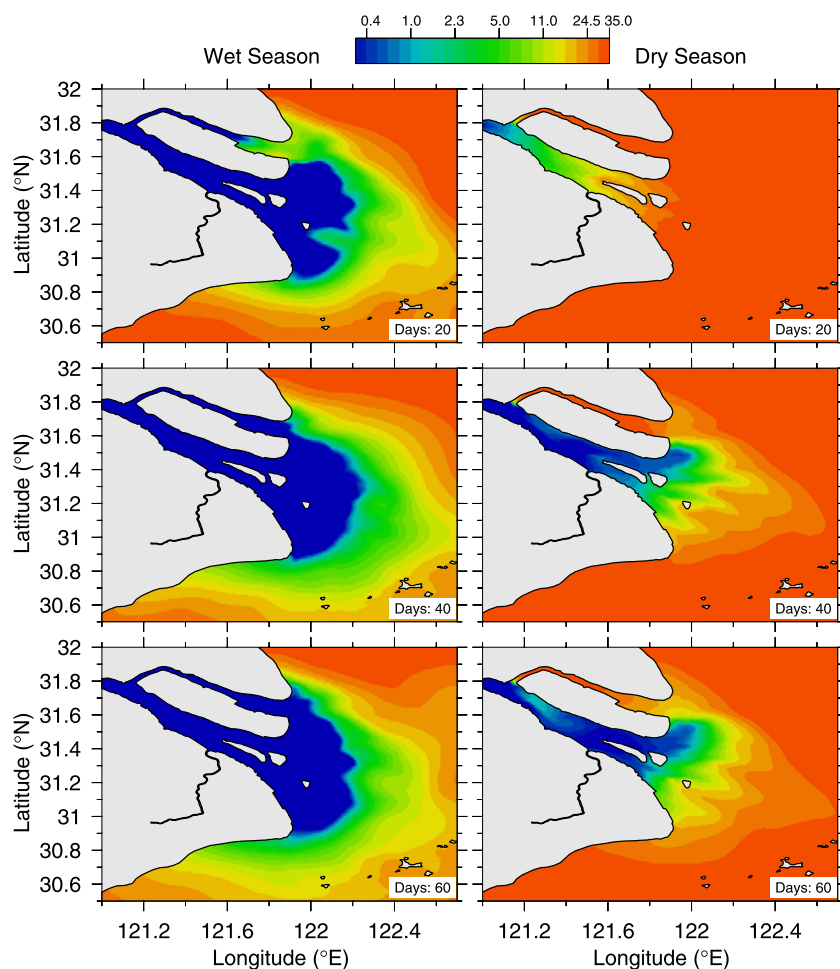


Figure 4. Distributions of the tidally averaged surface salinity for the model runs under the wet (left panels) and dry (right panels) season conditions on model days 20, 40, and 60.

the net water transport in the NB. To verify this hypothesis, we re-did Ex2 with a coarse model grid in the NB. The sensitivity analysis was done by comparing coarse and fine resolution model-predicted transports, with special focus on the need to resolve the intertidal zones in the NB around the northern end of Chongming Island for accurate transport estimation. The results obtained from this experiment can also provide a guide to evaluate previous model efforts in the CR.

3. Model Evidence of Saltwater Intrusion

[19] Given the same tidal forcing and background salinity, Ex1 and Ex2 show that model-predicted surface salinity distributions differ significantly during the wet and dry seasons. In the wet season, both the NB and SB are filled up rapidly by freshwater within a time scale of ~ 30 – 40 days (see the left panels in Figure 4), while in the dry season, although the SB is fully filled with freshwater within ~ 30 – 40 days, saltwater still remains in the NB after 60 days (see the right-hand panels in Figure 4). A counterclockwise return flow from the SB to the NB is evident along the southern tip of Chongming Island after 40 days during the dry season, which tends to reduce the salt in the downstream end of the NB during the dry season. At the same time, less saline water of <2 enters the SB along near the northern tip of Chongming

Island to form an isolated low-salinity bore in the western side of Chongming Island in the SB. This result agrees well with the observed salinity distribution shown in Figure 2. The anchor measurements detected the saltwater at Chongtong site in the SB, where the salinity was higher around this site than both upstream and downstream in this branch. Such a salinity distribution pattern is well reproduced by the model. The ship-survey measurements on the along-river transects from station 1 to station 21 showed that the saltwater was from the NB, with a maximum salinity of ~ 2 – 3 near where the NB separates from the SB. This feature is also resolved quantitatively by the model. A flux estimation made at the 60th model day shows a net upstreamward transport of $\sim 104 \text{ m}^3/\text{s}$ in the NB, which is the key process to cause the saltwater intrusion to the SB in this idealized dry season. These two experiments demonstrate that the saltwater intrusion is related to the amount of freshwater discharge. When it drops to $\sim 10,000 \text{ m}^3/\text{s}$ or less in the dry season, the NB acts as a barrier for the freshwater flowing from the upstream main river body and the saltwater in the NB can enter the SB on the northern tip of Chongming Island at the same time when the counterclockwise return flow appears around the southern tip of Chongming Island.

[20] In reality, the saltwater intrusion often occurs in winter after the transport adjustment from summer. Ex3 was

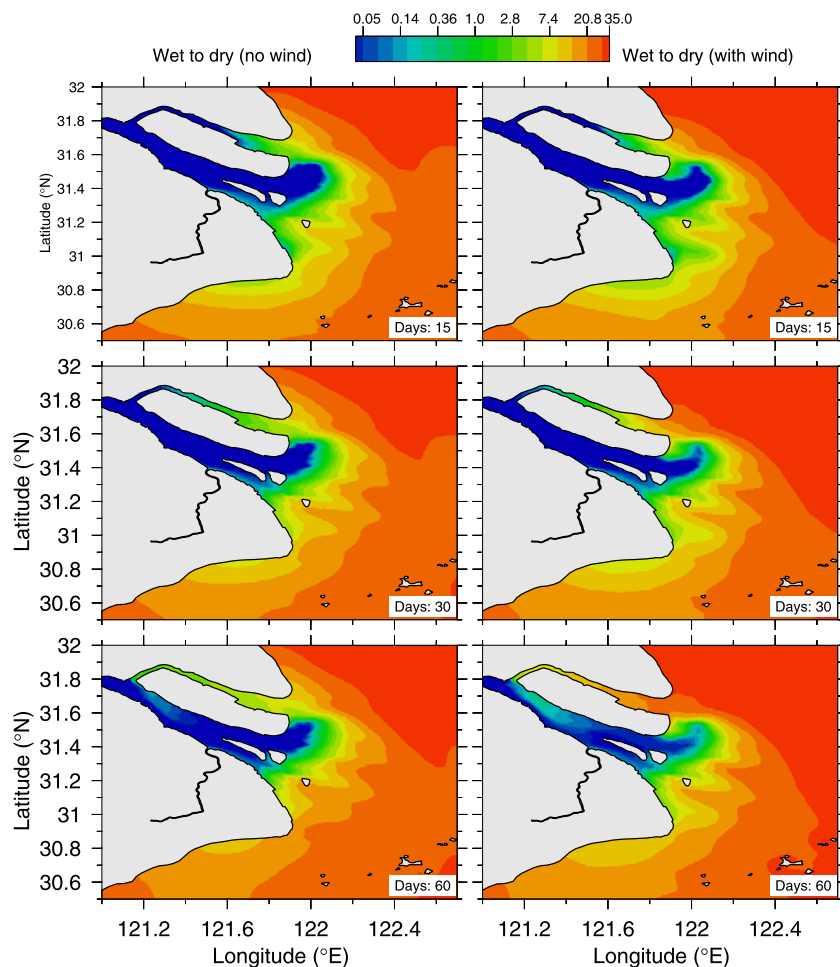


Figure 5. Distributions of the tidally averaged surface salinity for the model runs during and after the transition period from the wet season to the dry season on model days 15, 30, and 60. The left panels show the case without wind; the right panels show the case with a 5 m/s northerly wind.

designed to examine how the saltwater transport adjusts to the reduction in freshwater discharge rate from the wet season to the dry season. After the freshwater discharge rate decreases from $60,000 \text{ m}^3/\text{s}$ to $10,000 \text{ m}^3/\text{s}$, saltwater on the shelf is gradually pushed toward the CR (see the left panels in Figure 5). On the 15th model day, saltwater on the northern shelf off the CR enters the NB. This saltwater is advected northward in the NB and enters the SB along the northern tip of Chongming Island after 60 days. Two points are learned from Ex3. First, the saltwater intrusion from the shelf into the NB can occur in the dry season owing to a significant reduction of the river discharge. Second, the time scale of the salinity adjustment to produce the saltwater intrusion from the NB to the SB after the wet season is about 1–2 months.

[21] As a result of the monsoon climate in the East China Sea, northerly winds prevail in winter along the shelf off the CR. Ex4 examines the effect of the northerly wind on the saltwater intrusion. The northerly wind pushes the ocean water southward on the shelf but has little direct influence on the water movement inside the NB and SB. Blown by a northerly wind of 5 m/s (a southward wind stress of 0.036 N/m^2), more saltwater is advected into the NB as the oceanic water on the northern coast off the CR is pushed southward (see the

right panels in Figure 5). After 60 days, the entire NB is filled with relatively high-salinity water and the salinity concentration pumping into SB from the northern tip of Chongming Island could reach ~ 4.24 , significantly higher compared with a value of ~ 1.97 found in the case without wind. An unusually high salinity level of >3.5 was observed in SB in the 2004 hydrographic survey [He *et al.*, 2006], which was believed to be evidence of the effects of relatively strong northerly wind-forcing.

[22] The saltwater intrusion is also evident in the trajectories of Lagrangian particles. In the wet season, particles released in the upper part of the mainstream of the CR show a dominant group flowing through the SB and entering the shelf (see the top left panel in Figure 6). Although only one particle moves into the NB, it is symbolic of the outflow tendency of water movement in that branch during the wet season. This is supported by the trajectories of particles released near the mouth of the NB: all of them quickly leave the NB and move onto the shelf (see the top left panel in Figure 6). In the dry season, however, the particles released at the same upstream location of the CR all enter the SB and move toward the ocean, with several flowing into the NB by following the cyclonic flow around the southern end of

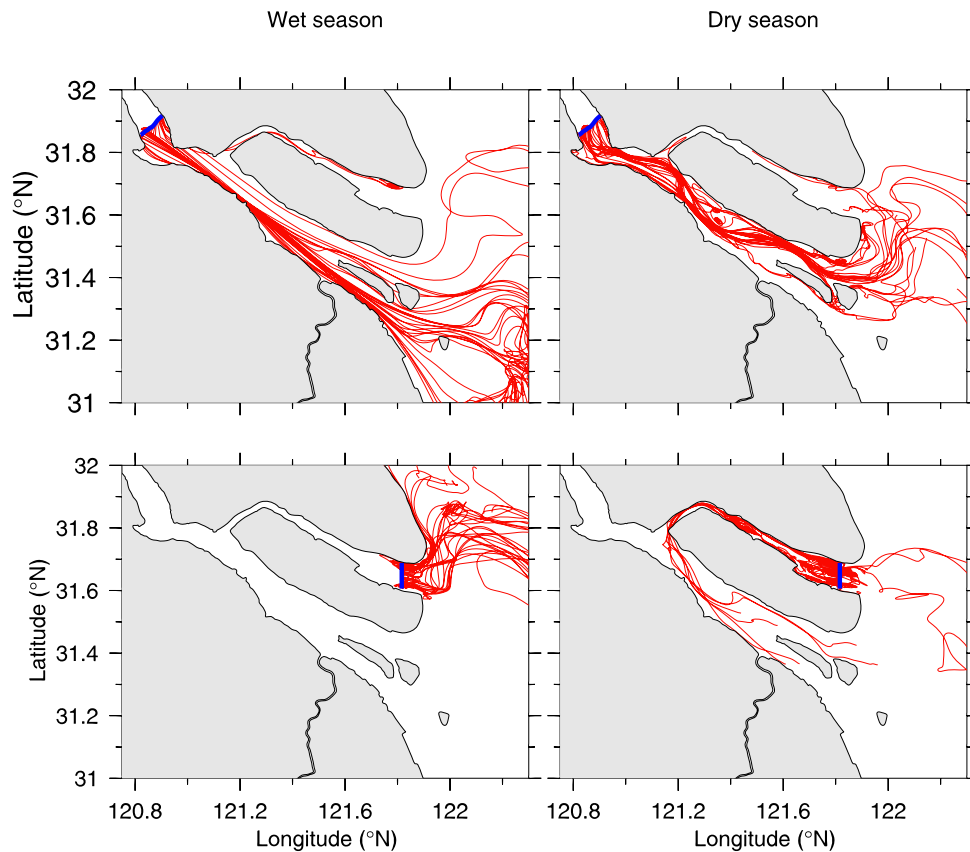


Figure 6. Subtidal trajectories of particles released on a cross-river section in the upstream region of the CR and near the mouth of the NB for the model run under the wet (left panels) and dry (right panels) season conditions. Particles were released after the subtidal currents in the NB reached an equilibrium state and tracked for 30 days.

Chongming Island (see the top right panel in Figure 6). Particles released near the mouth of the NB show a main group flowing upstream and then entering the SB from the northern tip of Chongming Island, although three of those particles move onto the shelf (see the top right panel in Figure 6). The trajectories of particles released in the dry season support our salinity simulation results and also demonstrate that the inflow to the NB can come from either the cyclonic return flow around the southern end of Chongming Island or saltwater inflow from the shelf.

[23] Particle trajectories shown in Figure 6 represent the advection of individual water parcels. Salt is a conservative tracer and the movement of a volume of this tracer is driven by the ensemble horizontal velocity and the concentration flux related to the vertical shear of the horizontal velocity of the tracer patch [Chen *et al.*, 2008b]. In an inhomogeneous flow field, movement of the tracer patch may differ significantly from trajectories of individual particles because it represents a continuous media and its movement is also influenced by vertical and lateral diffusion [Chen *et al.*, 2008b]. We next conducted a tracer experiment to examine the source of the inflow water in the NB during the dry season. When the tracer was released throughout the water column on a cross-branch section near the mouth of the NB after the residual flow in NB reached an equilibrium state in Ex2 (Figure 7), the tracer patch moved upstream, arriving at

the middle region of NB on day 5 and then entering the SB along the northern head of Chongming Island on day 10 (Figure 7). As more tracer flows into SB, it can occupy a larger portion of that branch. In this case, it only takes ~ 10 – 15 days for the tracer to travel from the mouth of the NB to the western tip of Chongming Island where the NB and SB originate. Unlike the Lagrangian particles released at the same location in the dry season (Figure 6), a significant amount of the tracer leaves the NB and enters the shelf, which, we believe, is owing to a combination of lateral dispersion and advection.

[24] To identify the source of the water flowing into the NB, we tracked the tracer released at the upstream region of the CR (Case A) and also on a cross-shelf section on the northern coast off the CR (Case B) for 30 days after the freshwater discharge drops from $60,000 \text{ m}^3/\text{s}$ to $10,000 \text{ m}^3/\text{s}$ in Ex3 (Figure 8). In Case A, the center of the tracer moves downstream along the SB, with most of the tracer spreading onto the shelf and a small portion ($\sim 1.6\%$) entering the NB around the southern end of Chongming Island. In Case B, although most of the tracer moves offshore, a small portion of the tracer ($\sim 1.1\%$) does enter the NB and move upstream. These two cases indicate that water in the NB can be supplied by two sources: (1) counterclockwise return flow around the southern end of Chongming Island, and (2) oceanic saltwater on the shelf. Lateral dispersion seems capable of advecting

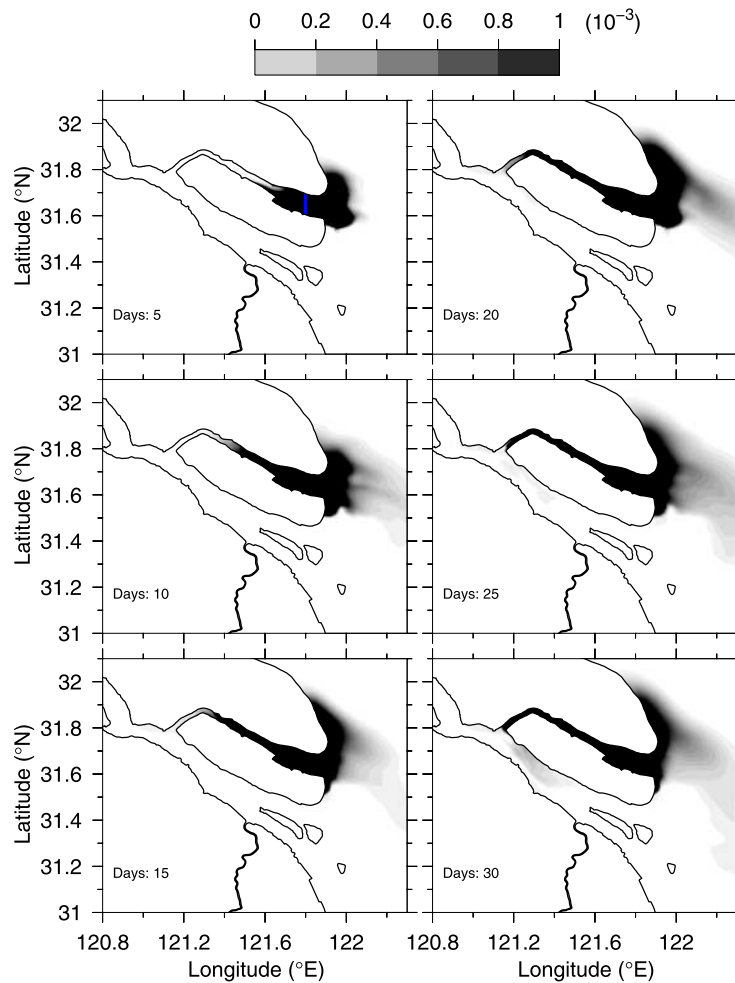


Figure 7. Distribution of the vertically averaged tracer concentration released on a section near the mouth of the NB for the model run under the dry season condition. The tracer was injected after the subtidal currents in the NB reached an equilibrium state and tracked for 30 model days. Heavy line is the location of the section where the tracer was injected.

tracer from the SB into the upper NB where the two branches originate. However, this dispersive flux is weakened by the upstream advection in the NB.

4. Physical Mechanism for Saltwater Intrusion

[25] The above process-oriented experiments show that with the same tidal forcing, the saltwater intrusion from the NB to the SB can occur during the dry season, and the amount of salt in the SB can be strongly influenced by the salinity of the inflow in the NB and the intensity of the northerly (downwelling-favorable) wind. It is clear that this intrusion is directly related to the decrease of freshwater discharge rate in the dry season, but it is unclear what is the specific physical process that generates a net flux from the NB to the SB. Considering the case with the only river discharge, we ran the model with freshwater discharge in the range of $10,000 \text{ m}^3/\text{s}$ to $80,000 \text{ m}^3/\text{s}$ in increments of $10,000 \text{ m}^3/\text{s}$. The percentage of freshwater entering the NB (hereafter referred to as PFRNB) can be approximately described by the regression function given as

$$\text{PFRNB} = 0.0001r^2 - 0.0005r + 0.0133, \quad (1)$$

where r is the freshwater discharge rate normalized by $10,000 \text{ m}^3/\text{s}$. PFRNB is 1.33% in the range of $10,000 \text{ m}^3/\text{s}$ to $40,000 \text{ m}^3/\text{s}$ and increases to 1.8% as r is increased to 8. If only river discharge rate is considered, the amount of freshwater entering NB is at a level of $\sim 133 \text{ m}^3/\text{s}$ in a dry season with a freshwater discharge rate of $10,000 \text{ m}^3/\text{s}$ and $\sim 834 \text{ m}^3/\text{s}$ in a wet season with a freshwater discharge rate of $60,000 \text{ m}^3/\text{s}$. This means that in order to cause a saltwater intrusion from the NB to the SB, the transport into the NB from the shelf and counterclockwise return flow around the southern end of Chongming Island must be larger than the discharge-induced flux in the dry and wet seasons, respectively.

[26] To examine the physical mechanisms governing the saltwater intrusion, we looked at the momentum balance under various forcing conditions and then studied the related transport process. The analysis was done on the NB cross-branch section (shown in red in Figure 1b) (hereafter referred to as section 1) where each term was directly computed using the FVCOM-CR time series output and averaged over a tidal cycle and in a cross-branch direction. We focused here on the along-branch component of the momentum balance since the NB is a narrow channel in which the along-branch Coriolis

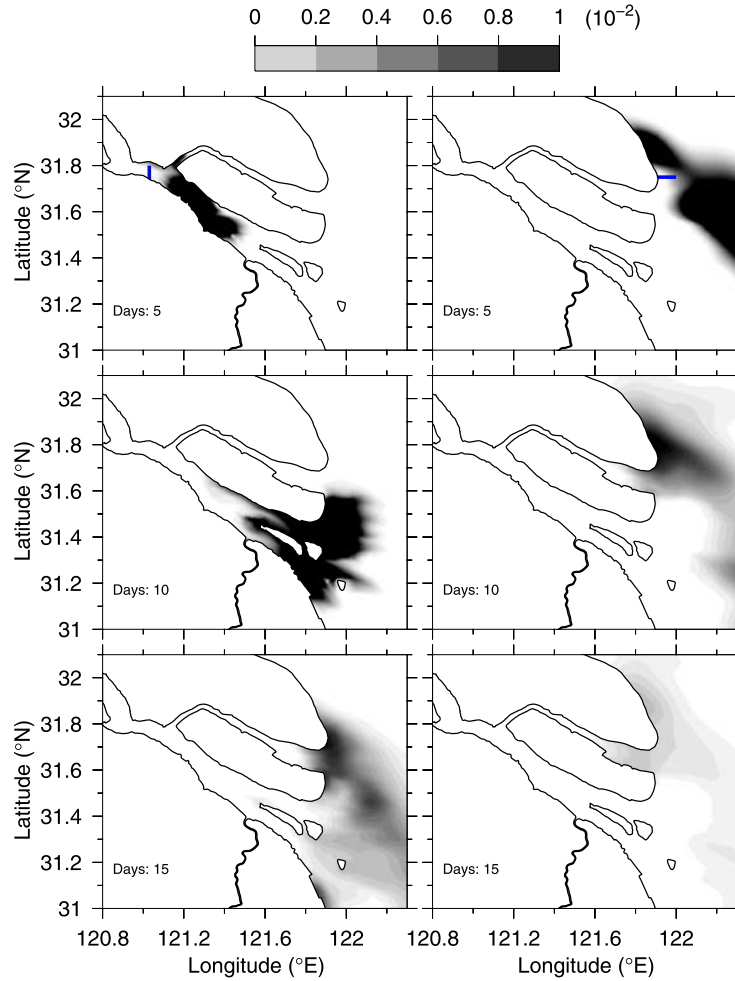


Figure 8. Distribution of the vertically averaged tracer concentration injected on two selected sections in the upstream area of the CR (left panels) and near the mouth of the NB (right panels) for the model run under the dry season condition. The tracer was injected at the same time as that shown in Figure 7 and also tracked for 30 model days. Heavy lines are the locations of the tracer injection.

force term is dynamically negligible and the other terms in this direction control the along-branch volume flux. Four cases are discussed here: (1) with only M_2 tidal forcing; (2) with M_2 tidal plus river discharge for the wet season; (3) with M_2 tidal plus river discharge for the dry season; and (4) with M_2 tidal plus river discharge for the dry season and a northerly wind of 5 m/s.

[27] For the case with only M_2 tidal forcing, the model shows that the along-branch residual flow is mainly driven by the resulting nonlinear advection, along-branch surface elevation gradient and vertical diffusion with the along-branch momentum balance given as

$$\begin{aligned} & \frac{1}{\Omega} \iint_{\Omega} (\vec{v} \cdot \nabla \vec{v})_l d\Omega + \frac{1}{\Omega} \iint_{\Omega} g \frac{\partial \zeta}{\partial l} d\Omega \\ & - \frac{1}{\Omega} \iint_{\Omega} \frac{\partial}{\partial z} \left(K_m \frac{\partial u_l}{\partial z} \right) d\Omega \\ & \sim 0, \end{aligned} \quad (2)$$

where the subscript l represents the component in the along-branch direction (positive in the seaward direction); \vec{v} is the

velocity vector; u_l is the long-branch component; ∇ is the gradient operator; K_m is the vertical eddy viscosity; ζ is the surface elevation; g is the gravitational acceleration; and Ω is the area of section 1; and the superscript “—” indicates tidal-cycle averaging. This balance remains unchanged from the surface to the bottom (Figure 9a) and with no wind stress applied in this case, the cross-section averaged transport is driven under a balance between the vertically integrated advection term, surface elevation gradient forcing and the bottom stress, a typical estuarine balance observed in many other estuaries [Grace, 1936; Bowden and Fairbairn, 1952; Friedrichs and Hamrick, 1996; Geyer et al., 2000; Winant and De Velasco, 2003] and suggested by other modeling estuarine and coastal analytical and numerical modeling experiments [Huthnance, 1973; Loder, 1980; Chen and Beardsley, 1995, Chen et al., 2008c; Zheng et al., 2003].

[28] In this only tidal forcing case, the residual current is driven by two distinct mechanisms. The first mechanism is produced by the nonlinear relationship between currents and surface elevation. Since the surface elevation gradient decreases seaward, this mechanism tends to push the water flow from the NB to the ocean. The second mechanism is

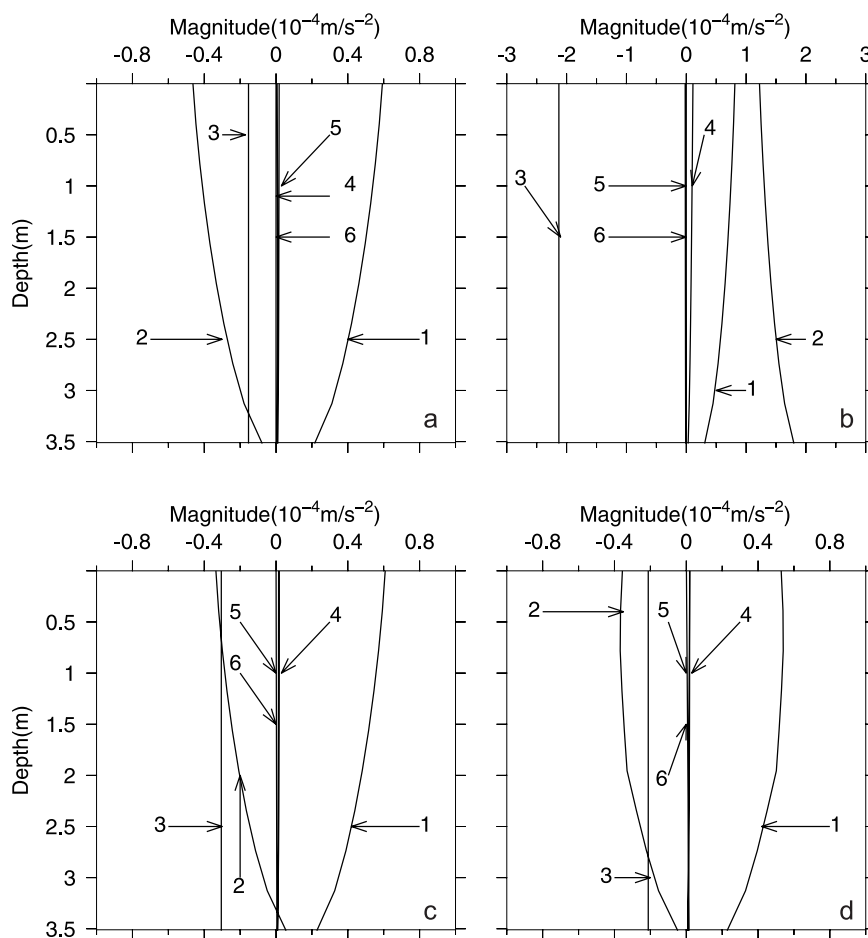


Figure 9. Vertical profile of each term in the along-branch component of the momentum equation on section 1 for the cases with (a) only tide, (b) wet season, (c) dry season with no wind, and (d) dry season with wind. Each profile is identified as follows: (1) advection $((1/\Omega)\int_{\Omega}(\vec{v}\cdot\nabla\vec{v})d\Omega)$; (2) vertical diffusion $(-(1/\Omega)\int_{\Omega}(\partial/\partial z)(K_m(\partial u_i/\partial z))d\Omega)$; (3) surface elevation gradient $((1/\Omega)\int_{\Omega}g(\partial\zeta/\partial l)d\Omega)$; (4) horizontal diffusion term; (5) Coriolis term; and (6) baroclinic pressure gradient. Section location is shown in Figure 1.

so-called tidal rectification, which is caused mainly by nonlinear advection and vertical diffusion. In our case, this mechanism produces a landward transport from the NB to the SB. These two mechanisms are similar to that found in the current measurements by *Friedrichs and Hamrick* [1996], except that the tidal rectification found in the NB shows an opposite role in the water transport than what they reported. The residual currents do show numerous eddy-featured patterns in the NB, which are generated by the interaction of tidal currents with local topography like those described in the work of *Li et al.* [2008] and *Chen et al.* [2008c] rather than the reverse current pattern found by *Li and O'Donnell* [1997] in a long closed estuary (flowing landward over the shoal and returned seaward in the channel) and by *Li and O'Donnell* [2005] in a short closed estuary (flowing seaward over the shoal and returning landward in the channel). In our case here, the tidal rectification produces a net upstream volume flux of $288\text{ m}^3/\text{s}$ through the NB at section 1. This means that if there were no freshwater discharge from the upstream of CR, there would always be a net water transport from the NB to the SB. Therefore, in order to suppress the saltwater intrusion from the NB, the freshwater transport entering the

NB must be equal to or larger than this tidal rectification transport. For this case, the criterion value is $288\text{ m}^3/\text{s}$. Assuming a linear dynamical system, one can simply combine the transports determined by the cases with only river discharge and tidal forcing, which suggests a saltwater intrusion in the dry season because the river discharge transport into the NB is smaller than the tidal rectification transport. Since the dynamics in the NB, however, are fully nonlinear, the momentum balance in a system with river discharge, tides and winds is more complex than linear superposition.

[29] For the case with the river discharge of $60,000\text{ m}^3/\text{s}$ (the wet season), the along-branch residual current in the NB is driven with the same dominant momentum balance being among the nonlinear advection, surface elevation gradient forcing and vertical diffusion terms shown in (2). In such a shallow NB, even in the wet season, the baroclinic pressure gradient is orders of magnitude smaller than either of three terms in (2), so its contribution can be neglected (Figure 9b). In this case, the surface elevation gradient forcing remains seaward, with a much higher value than that shown in the case with the only M_2 tide. This forcing always acts as a force

to push the water out of the NB to the shelf. From (2), we see that the residual flow is driven by the two interaction mechanisms described in the case with the only tidal forcing except that the relative contribution of these three terms changes. Since the surface elevation gradient forcing-driven flow (seaward) is larger than rectification flow (landward), a saltwater intrusion cannot happen.

[30] In this wet season case, the model predicts a net flux of $\sim 1340 \text{ m}^3/\text{s}$ entering the NB at the northern end of Chongming Island and flowing onto the shelf. This flux is $506 \text{ m}^3/\text{s}$ larger than the transport of $834 \text{ m}^3/\text{s}$ predicted by the regression function (1) for the case with only river discharge. In the case with only tidal forcing, we show that tidal rectification can cause a net flux of $\sim 288 \text{ m}^3/\text{s}$ from the NB to the SB around the northwestern end of Chongming Island. The fact that a net flux entering the NB is significantly larger than the water transport driven by the pure discharge charge suggests that the resulting the surface elevation gradient forcing, advection and bottom friction tends to enhance the outflow from the NB to the shelf during the wet season. This is also evident in the sign of the vertical diffusion term in the momentum balance. It is positive in the case with only M_2 tidal forcing but negative in the case with tide plus the wet season river discharge.

[31] For the case with a river discharge of $10,000 \text{ m}^3/\text{s}$ (the dry season), the along-branch residual current in the NB is also driven mainly by the momentum balance among the nonlinear advection, surface elevation gradient forcing and vertical diffusion terms described in (2). It is clear that the physical mechanism driving the net flux into the NB remains the same for the dry and wet seasons, but the roles of these key processes significantly differ in these two cases. This can be seen in the difference in sign and magnitude of each term in the momentum balance equation. In the dry season case, the surface elevation gradient forcing is much smaller and the vertical diffusion term is positive throughout the water column except in the bottom sigma layer (Figure 9c). Although the surface elevation gradient forcing is smaller in the dry season case, the surface elevation is still higher in the upstream area than in the downstream area, so that this forcing acts the same as in the wet season case to push the water out of the NB to the shelf. Since the saltwater intrusion occurs in this case and the baroclinic pressure gradient is too small to be taken into account, the saltwater intrusion is driven by the rectification resulting from the nonlinear interaction of the surface elevation gradient, bottom stress, and advection.

[32] In this dry season case, the model predicts a net flux of $\sim -104 \text{ m}^3/\text{s}$ from the NB to the SB through the section around the northwestern end of Chongming Island. This value is about $51 \text{ m}^3/\text{s}$ smaller than a resulting transport of $155 \text{ m}^3/\text{s}$ determined by a linear combination of the transports predicted by the river discharge and tidal forcing separately. The fact is that the signs of advection, surface elevation gradient forcing and vertical diffusion terms in most of the water column are the same in the cases for the dry season and only M_2 tidal forcing. This suggests that as the surface elevation gradient decreases from the wet season to the dry season, tidal rectification becomes a dominant mechanism driving the landward water transport in the NB.

[33] For the case with a river discharge of $10,000 \text{ m}^3/\text{s}$ (the dry season) plus a northerly wind of 5 m/s , the key processes

controlling the along-branch residual current remain the same as the dry season case without the wind (Figure 9d). The wind-induced mixing slightly increases the magnitude of the vertical diffusion term and decreases the magnitude of the advection term. The mixing also decreases the vertical shear of the advection and vertical diffusion terms in the upper 2 m of the water column below the sea surface. The big difference is in the surface elevation gradient forcing term, which drops from $\sim 0.3 \times 10^{-4} \text{ m/s}^2$ without wind to $\sim 0.2 \times 10^{-4} \text{ m/s}^2$ with wind. Since the surface elevation is always higher in the upstream area than in the downstream area and the surface elevation gradient forcing is a key forcing to restrict the saltwater intrusion, it is clear that reducing the magnitude of this forcing can enhance the saltwater intrusion in the dry season.

[34] In this wind case, the model predicts the net flux of $\sim 117 \text{ m}^3/\text{s}$, which is about $13 \text{ m}^3/\text{s}$ larger than the case without wind. It is clear from the momentum balance that the increase in the transport in the wind case is due to the decrease of the seaward surface elevation gradient forcing rather than either the baroclinic pressure gradient forcing or the wind-driven Ekman transport. The baroclinic pressure gradient forcing is too small to be taken into account in the NB. Although a northerly wind of 5 m/s (with a wind stress of 0.036 N/m^2) can produce the landward Ekman transport of $\sim 3500 \text{ m}^3/\text{s}$ across the branch width of 10 km over the shelf, it is not applicable for the NB of the CR, because the Coriolis force is a negligible term within the NB and the response of the water current to the wind in a shallow estuarine region does not follow simple Ekman theory.

[35] It should be pointed out here that the spatial distribution and magnitude of the residual currents differ greatly in the wet and dry seasons. In the wet season, both the SB and NB are dominated by outflow, even though the currents are much weaker in the NB than in the SB (Figure 10a). For a given freshwater discharge rate of $60,000 \text{ m}^3/\text{s}$, 2.2% ($1340 \text{ m}^3/\text{s}$) enters the NB while 97.8% ($58,660 \text{ m}^3/\text{s}$) remains in the SB. In the dry season, however, SB is still the primary outflow conduit, but the NB is characterized by a more complex flow pattern (Figure 10b). For a given freshwater discharge rate of $10,000 \text{ m}^3/\text{s}$, there is a net flux of $104 \text{ m}^3/\text{s}$ from the NB to the SB, which increases the volume flux in the SB to $10,104 \text{ m}^3/\text{s}$.

5. Discussion

[36] FVCOM-CR successfully reproduces the saltwater intrusion through the NB into the SB. The freshwater discharge versus tidal rectification mechanism proposed here suggests that in order to quantify the level of the intrusion, we need to accurately simulate the water transport using a fully nonlinear dynamical system approach. Since local bathymetry and coastline geometry are very complex, a mass conservative unstructured-grid model like FVCOM is ideal. A fundamental issue is raised in applying FVCOM to the CR: What is the appropriate model resolution required for this system? To address this issue, one needs to run the model in a convergence experiment with various horizontal resolutions. In general, the numerical convergence rate also depends on local bathymetry, so that the need for horizontal resolution varies with bathymetry, thus a convergence experiment is defined relative to given bathymetry. Since the CR features

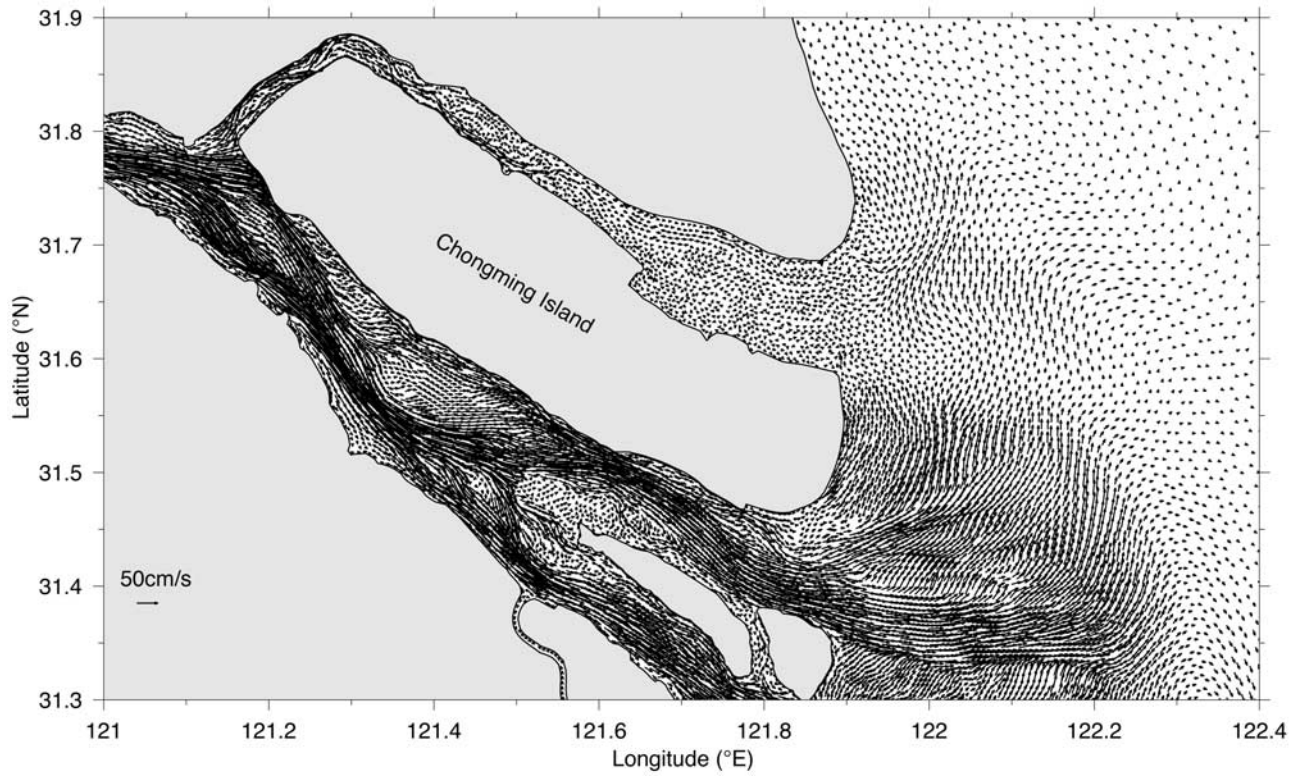


Figure 10a. Distribution of the vertically averaged residual current for the model run under the wet season condition after a 60-day model integration.

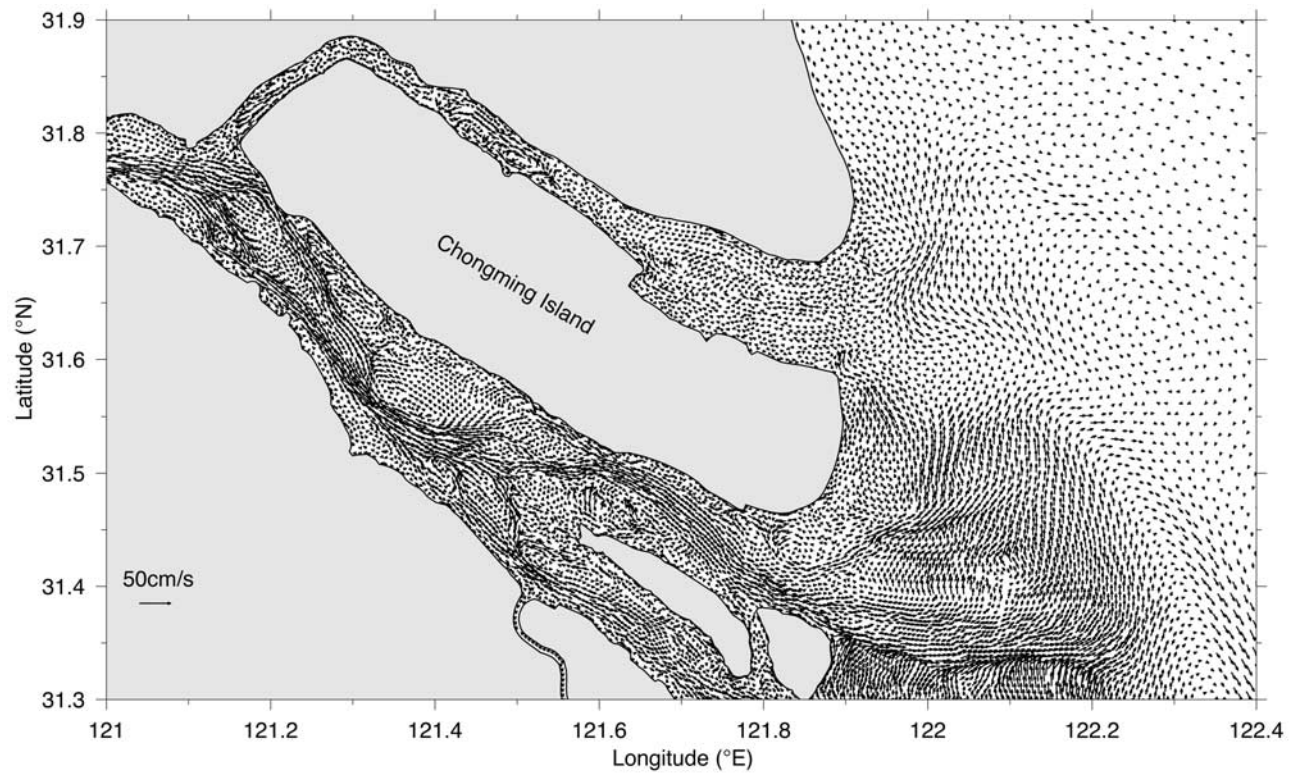


Figure 10b. Distribution of the vertically averaged residual current for the model run under the dry season condition after a 60-day model integration.

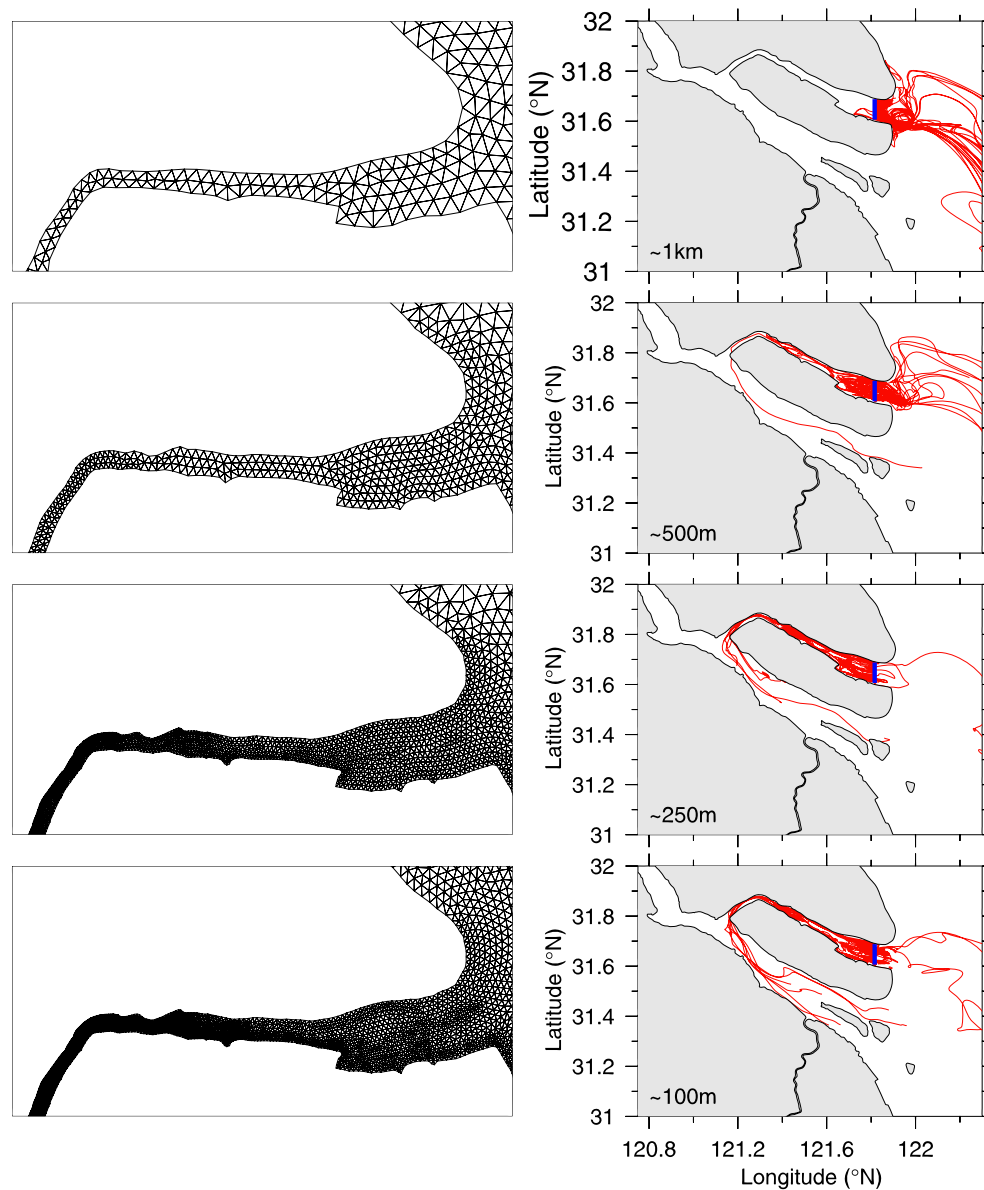


Figure 11. Unstructured grid in the NB (left panels) and subtidal trajectories of particles (right panels) for the model runs with horizontal resolutions of ~ 1.0 , 0.75 , 0.5 , 0.25 , and 0.1 km in the dry season condition. The particles were released at the same time as shown in Figure 6 and also tracked for 30 days.

large deposits of suspended sediment, the bathymetry may vary on both short-term (after a storm passed) and long-term (seasonal sedimentation) time scales. The bathymetry data available for this research have a spatial resolution of ~ 100 m and FVCOM-CR was configured with a horizontal resolution compatible with this given bathymetry. Although we are unable to determine an optimal grid for numerical convergence to a realistic CR owing to variability in the bathymetry, we can still examine whether or not our model simulation results are sensitive to the spatial model resolution with the prerequisite for coastal geometric fitting.

[37] For the given bathymetry data, we have conducted a sensitivity experiment with horizontal resolutions of ~ 1.0 , 0.75 , 0.5 , 0.25 and 0.1 km in the NB for Ex2. In this dry season experiment, the tidal and river discharge forcing are the same. The model results clearly show that water transport

through the NB varies significantly with model spatial resolution. In the case with horizontal resolution of ~ 1 km, water transport into the NB at its entrance increased, which caused the net outflow from the NB to the shelf to be $108 \text{ m}^3/\text{s}$. When the horizontal resolution was refined to ~ 0.5 km, the net transport through the NB reversed, but its value is very small. The net transport through the NB into the SB increased to $-79 \text{ m}^3/\text{s}$ when the horizontal resolution was reduced to ~ 0.25 km, and reached an equilibrium value of $-104 \text{ m}^3/\text{s}$ after the horizontal resolution was reduced to ~ 0.1 km or less. This process can be seen in the Lagrangian trajectories of particles released on the section near the mouth of the NB (Figure 11), in which all particles outflow to the shelf in the 1-km resolution case, a few particles move upstream in the 0.5-km resolution case, and most particles flow upstream and enter the SB through the narrow channel on the northern head

of Chongming Island in the 0.25- and 0.1-km resolution cases.

[38] This sensitivity analysis suggests that the critical need for horizontal resolution is to resolve accurately the details in the narrow channel of the NB around the northern end of CI. Failure to do this can overestimate water transport into the NB from the mainstream of the CR, and thus eliminate the saltwater intrusion.

6. Summary and Conclusions

[39] The high-resolution FVCOM-CR accurately simulates the saltwater intrusion into the CR that often occurs in the dry season. The mechanism analysis suggests that the intrusion results from a complex nonlinear interaction process of tidal currents, surface elevation gradient forcing, and vertical diffusion. The tidal rectification, resulting from the nonlinear interaction of tidal currents and bottom friction over abrupt topography, produces a net upstreamward volume flux from the NB to the SB. The saltwater intrusion occurs when the freshwater flow into the NB is smaller than the tidal rectified flow. In the wet season, the surface elevation gradient forcing is sufficiently large to maintain the transport into the NB. This inflow is driven through an along-branch momentum balance between the surface elevation gradient forcing, nonlinear current advectations and bottom friction. In the dry season, reducing the surface elevation gradient forcing makes tidal rectification becomes a key process favorable for the saltwater intrusion. The fact that the model-predicted net flux of the saltwater intrusion is smaller than the sum of the freshwater discharge and tidal rectified transports in the NB suggests that the resulting surface elevation gradient forcing, tidal rectified flow and vertical diffusion tends to reduce an upstreamward flux. A northerly wind tends to enhance the saltwater intrusion by reducing the seaward surface elevation gradient forcing rather than either by the baroclinic pressure gradient forcing or local wind-driven Ekman transport. Both the baroclinic pressure gradient and the Coriolis force are negligible terms in the momentum equation within the CR and the transport entering the NB from the shelf does not follow simple Ekman theory.

[40] For the available bathymetry data, the convergence numerical solution of FVCOM-CR is reached as the horizontal resolution becomes compatible to the bathymetry resolution. A convergence experiment suggests that in order to correctly resolve the net transport through the NB in the dry season, a high-resolution grid (~ 100 m or less) is required in the narrow channel around the northern head of Chongming Island.

[41] We note here that this work was conducted using idealized forcing cases that represent the climatology in the wet and dry seasons and focused on the physical mechanism for the cause of the saltwater intrusion. A realistic simulation requires the accurate initial condition of water salinity and realistic meteorological and tidal forcing as well as river discharge rate. In addition, the geography at the mouth of the CR changes with time as a result of sedimentation and other human construction. These factors must be taken into account when a realistic simulation is proposed.

[42] **Acknowledgments.** The development of FVCOM is supported by the Massachusetts Fisheries Institute through NOAA grants DOC/NOAA/NA04NMF4720332 and DOC/NOAA/NA05NMF4721131; NSF

grants OCE-0234545, OCE-0227679, OCE-0606928, OCE-0712903, OCE-0732084, OCE-0726851, ARC0712903; ARC0732084, and ARC0804029; NOAA grant NA160P2323; and an ONR subcontract grant from the Woods Hole Oceanographic Institution. The development of the nested modeling approach is supported by MIT and URI Sea Grant projects NA060AR41700019 and R/P-061. C. Chen serves as Zi Jiang Scholar at the State Key Laboratory for Estuarine and Coastal Research, East China Normal University (ECNU), and is an adjunct professor at Shanghai Ocean University (SHOU). His contribution is also supported by both ECNU and SHOU. P. Ding is supported by the Chinese National Key Basic Research Project grant 2002CB412403. This paper is 08–1101 in the SMAST Contribution Series, School of Marine Science and Technology, University of Massachusetts, Dartmouth. We would like to thank Chunyan Li, Louisiana State University, for providing a detailed description and explanation of his and O'Donnell's previous theoretical work on tidally driven flows in idealized semienclosed estuaries, and also the FVCOM team members G Cowles, J. Qi, Q. Xu, D. A. Stuebe, and L. Zhao for their help in using FVCOM. Comments from two anonymous reviewers also helped improve this paper.

References

- Beardsley, R., R. Limeburner, H. Yu, and G. A. Cannon (1985), Discharge of the Changjiang (Yangtze River) into the East China Sea, *Cont. Shelf Res.*, *4*, 57–76, doi:10.1016/0278-4343(85)90022-6.
- Bowden, K. F., and L. A. Fairbairn (1952), A determination of the frictional forces in a tidal current, *Proc. R. Soc. London, Ser. A*, *214*, 371–392, doi:10.1098/rspa.1952.0175.
- Burchard, H. (2002), *Applied Turbulence Modeling in Marine Waters, Lecture Notes in Earth Sci.*, vol. 100, 215 pp., Springer, New York.
- Chen, C., and R. C. Beardsley (1995), A numerical study of stratified tidal rectification over finite-amplitude banks. part 1: Symmetric banks, *J. Phys. Oceanogr.*, *25*, 2090–2110, doi:10.1175/1520-0485(1995)025<2090:ANSOST>2.0.CO;2.
- Chen, C., R. Beardsley, and R. Limeburner (1994), Comparison of winter and summer hydrographic observations in the Yellow and East China Seas and adjacent Kuroshio during 1986, *Cont. Shelf Res.*, *14*, 909–929, doi:10.1016/0278-4343(94)90079-5.
- Chen, C., H. Liu, and R. Beardsley (2003), An unstructured grid, finite-volume, three dimensional, primitive equations ocean model: Application to coastal ocean and estuaries, *J. Atmos. Oceanic Technol.*, *20*(1), 159–186, doi:10.1175/1520-0426(2003)020<0159:AUGFVT>2.0.CO;2.
- Chen, C., R. C. Beardsley, and G. Cowles (2006a), An unstructured grid, finite-volume coastal ocean model (FVCOM) system, *Oceanography*, *19*(1), 78–89.
- Chen, C., G. Cowles, and R. C. Beardsley (2006b), An unstructured grid, finite-volume coastal ocean model: FVCOM user manual, 2nd ed., *Tech. Rep. 06-0602*, 315 pp., Sch. For Mar. Sci., Univ. of Mass., Dartmouth, Mass.
- Chen, C., H. Huang, R. C. Beardsley, H. Liu, Q. Xu, and G. Cowles (2007), A finite-volume numerical approach for coastal ocean circulation studies: Comparisons with finite difference models, *J. Geophys. Res.*, *112*, C03018, doi:10.1029/2006JC003485.
- Chen, C., et al. (2008a), Physical mechanisms for the offshore detachment of the Changjiang diluted water in the East China Sea, *J. Geophys. Res.*, *113*, C02002, doi:10.1029/2006JC003994.
- Chen, C., Q. Xu, R. W. Houghton, and R. C. Beardsley (2008b), A model-dye comparison experiment in the tidal mixing front zone on the southern flank of Georges Bank, *J. Geophys. Res.*, *113*, C02005, doi:10.1029/2007JC004106.
- Chen, C., J. Qi, C. Li, R. C. Beardsley, H. Lin, R. Walker, and K. Gates (2008c), Complexity of the flooding/drying process in an estuarine tidal-creak salt-marsh system: An application of FVCOM, *J. Geophys. Res.*, *113*, C07052, doi:10.1029/2007JC004328.
- Friedrichs, C. T., and J. M. Hamrick (1996), Effects of channel geometry on cross sectional variations in along channel velocity in partially stratified estuaries, in *Buoyancy Effects on Coastal and Estuarine Dynamics, Coastal and Estuarine Stud.*, vol. 53, edited by D. G. Aubrey and C. T. Friedrichs, pp. 283–300, AGU, Washington, D.C.
- Geyer, W. R., J. H. Trowbridge, and M. M. Bowen (2000), The dynamics of a partially mixed estuary, *J. Phys. Oceanogr.*, *30*, 2035–2048, doi:10.1175/1520-0485(2000)030<2035:TDOAPM>2.0.CO;2.
- Grace, S. (1936), Friction in the tidal currents of the Bristol Channel, *Mon. Not. R. Astron. Soc.*, *3*, 388–395.
- He, S. L., P. X. Ding, and Y. Z. Kong (2006), Salinity variation in the southern branch and salt water intrusion in the northern branch of the Changjiang, *Adv. Nat. Sci.*, *16*(5), 584–589.
- Huthnance, J. M. (1973), Tidal current asymmetries over the Norfolk Sandbank, *Estuarine Coastal Mar. Sci.*, *1*, 89–99, doi:10.1016/0302-3524(73)90061-3.

- Kobayashi, M. H., J. M. C. Pereira, and J. C. F. Pereira (1999), A conservative finite-volume second-order-accurate projection method on hybrid unstructured grids, *J. Comput. Phys.*, *150*, 40–45, doi:10.1006/jcph.1998.6163.
- Kong, Y. Z., S. L. He, P. X. Ding, and K. L. Hu (2004), Characteristics of temporal and spatial variation of salinity and their indicating significance in the Changjiang estuary, *Acta Oceanol. Sin.*, *26*(4), 9–18.
- Li, C., and J. O'Donnell (1997), Tidally driven residual circulation in shallow estuaries with lateral depth variation, *J. Geophys. Res.*, *102*, 27,915–27,929, doi:10.1029/97JC02330.
- Li, C., and J. O'Donnell (2005), The effect of channel length on the residual circulation in tidally dominated channels, *J. Phys. Oceanogr.*, *35*, 1826–1840, doi:10.1175/JPO2804.1.
- Li, C., C. Chen, D. Guadagnoli, and I. Y. Georgiou (2008), Geometry induced residual eddies in estuaries with curved channel-observations and modeling studies, *J. Geophys. Res.*, *113*, C01005, doi:10.1029/2006JC004031.
- Li, T., Y. Li, X. Gao, and Y. Wang (2005), Effects of regulation project on salinity intrusion in Yangtze Estuary, *Ocean Eng.*, *23*, 31–38.
- Loder, J. W. (1980), Topographic rectification of tidal currents on the sides of Georges Bank, *J. Phys. Oceanogr.*, *10*, 1399–1416, doi:10.1175/1520-0485(1980)010<1399:TROTCO>2.0.CO;2.
- Luo, X., and Z. Chen (2005), Numerical simulation study of effect of runoff and tide on the Changjiang River mouth saltwater intrusion, *Coastal Eng.*, *24*, 1–6.
- Luo, X., and Z. Chen (2006), Analysis of salinity's variation in the North Channel of the Yangtze Estuary, *Port Waterw. Eng.*, *11*, 79–82.
- Ma, G., S. Liu, and D. Qi (2006), Three dimensional hydrodynamic model of Yangtze Estuary, *J. Hydrodyn.*, *21*, 53–61.
- Mao, Z. C., and H. Shen (1995), Study on type of saltwater intrusion for tidal branching: A case study on Changjiang estuary, *J. East China Normal Univ.*, *2*, 77–85.
- Mao, Z. C., H. Shen, and C. Xiao (2001), Saltwater intrusion patterns in the Qingchaosha area, Changjiang River Estuary, *Oceanol. Limnol. Sin.*, *32*, 58–66.
- Mellor, G. L., and T. Yamada (1982), Development of a turbulence closure model for geophysical fluid problem, *Rev. Geophys. Space Phys.*, *20*, 851–875, doi:10.1029/RG020i004p00851.
- Pietrzak, J. J., B. Jakobson, H. Burchard, H. J. Vested, and O. Petersen (2002), A three-dimensional hydrostatic model for coastal and ocean modeling using a generalized topography following co-ordinate system, *Ocean Modell.*, *4*, 173–205, doi:10.1016/S1463-5003(01)00016-6.
- Smagorinsky, J. (1963), General circulation experiments with the primitive equations, I. The basic experiment, *Mon. Weather Rev.*, *91*, 99–164, doi:10.1175/1520-0493(1963)091<0099:GCEWTP>2.3.CO;2.
- Winant, C. D., and G. G. De Velasco (2003), Tidal dynamics and residual circulation in a well-mixed inverse estuary, *J. Phys. Oceanogr.*, *33*, 1365–1379, doi:10.1175/1520-0485(2003)033<1365:TDArcI>2.0.CO;2.
- Wu, H., and J. Zhu (2007), Analysis of the transport mechanism of the saltwater spilling over from the north branch in the Changjiang Estuary in China, *Acta Oceanol. Sin.*, *29*, 17–25.
- Xiao, C., and H. Shen (1998), The analysis of factors affecting on the saltwater intrusion in Changjiang Estuary, *Huadong Shifan Daxue Xuebao*, *3*, 74–80.
- Xiao, C., J. Zhu, and H. Shen (2000), Study of numerical modelling about saltwater flow backward in the Changjiang Estuary, North Branch, *Acta Oceanol. Sin.*, *22*, 125–132.
- Zheng, L., C. Chen, and H. Liu (2003), A modeling study of the Satilla River Estuary, Georgia. part I: Flooding/drying process and water exchange over the salt marsh-estuary-shelf complex, *Estuaries*, *26*(3), 651–669, doi:10.1007/BF02711977.

R. C. Beardsley, Department of Physical Oceanography, Woods Hole Oceanographic Institution, Woods Hole, MA 02543, USA. (rbeardsley@whoi.edu)

C. Chen, H. Lin, and P. Xue, School for Marine Science and Technology, University of Massachusetts-Dartmouth, New Bedford, MA 02744, USA. (c1chen@umassd.edu; hlin@umassd.edu; pxue@umassd.edu)

P. Ding, J. Ge, and Y. Kong, State Key Laboratory for Estuarine and Coastal Research, East China Normal University, Shanghai 200062, China. (pxding@sklec.ecnu.edu.cn; jzge@sklec.ecnu.edu.cn; yzkong@sklec.ecnu.edu.cn)